Journal of Nuclear Materials 407 (2010) 119–125

Contents lists available at ScienceDirect

Journal of Nuclear Materials

journal homepage: www.elsevier.com/locate/jnucmat

Letter to the Editor

Phase-field modeling of void migration and growth kinetics in materials under irradiation and temperature field

Yulan Li *, Shenyang Hu, Xin Sun, Fei Gao, Charles H. Henager Jr., Mohammad Khaleel

Pacific Northwest National Laboratory, 902 Battelle Boulevard, Richland, WA 99352, USA

ARTICLE INFO

Article history:
Received 10 May 2010
Accepted 27 September 2010

ABSTRACT

A phase-field model is developed to investigate the migration of vacancies, interstitials, and voids during irradiation in a thermal gradient. Void growth kinetics during irradiation are also modeled. The model accounts for the generation of defects including vacancies and interstitials associated with the radiation damage, recombination of vacancies and interstitials, defect diffusion, and defect sinks. The effect of void size, vacancy concentration, vacancy generation rate, recombination rate, and temperature gradient on a single void migration and growth is parametrically studied. The results demonstrate that a temperature gradient causes void migration and defect fluxes, i.e., the Soret effect, which affects void stability and growth kinetics. It is found that (1) void migration mobility is independent of void size, which is in agreement with the theoretical prediction under the assumption of bulk diffusion controlled migration; (2) void migration mobility strongly depends on the temperature gradient and (3) the effect of defect concentration, generation rate, and recombination rate on void migration mobility is minor although they strongly influence void growth kinetics.

Published by Elsevier B.V.

1. Introduction

Vacancies and interstitials are two major defects produced by high-energy fission fragments and neutrons in nuclear reactor components, such as nuclear fuels and cladding materials. With the accumulation of these defects, void nucleation, growth, and volume swelling take place. A complex void microstructure is often observed in both nuclear fuels and cladding materials [1–5], including inhomogeneous void size, shape, and spatial distributions. In addition, in the presence of temperature gradients, voids can migrate. It is believed that the observed formation of central holes in spent nuclear fuels results from the migration of voids [5,6]. Since the thermo-mechanical properties [7–11], including thermal conductivity, ductility, and creep properties as well as structural instabilities such as volume swelling and cracking, strongly depend on the microstructure, it is desired to develop predictive simulation tools for investigating the kinetics of microstructure evolution for modeling the performance of nuclear reactor components. In turn, these microstructural simulation tools could be used to provide the fundamental thermodynamic and kinetic databases of irradiated materials for more macroscopic simulations.

Different theoretical models are employed to study void migration since it was first observed [12–19]. Shewmon [15] theoretically investigated void mobility via vacancy diffusion. Perryman and Goodhew [16] developed a theoretical model to describe the migration of voids and the growth of void populations. Tikare and Holm [17] used a statistical–mechanical model (the Potts Monte Carlo method) to simulate simultaneous grain growth and void migration with the assumption that surface diffusion dominates the void migration. Recently, Hu and Henager [20] developed a phase-field model to simulate void migration in a temperature field. However, none of these models considered the effect of radiation on void migration and growth kinetics.

The phase-field method, seen as a unique mesoscale simulation approach, has been extensively applied to predict microstructures and their evolution kinetics in important materials processes such as solidification [21], ferroelectric transition [22], phase-separation and precipitation [23], martensitic transition [24], dislocation dynamics [25], gas bubble and void evolution in nuclear materials [20,26–30], elastic–plastic deformation [31,32], and crack propagation [33]. In the present work we extend the phase-field model [20] to study the effect of both temperature gradients and radiation on void migration and void evolution kinetics. The generation of vacancies and interstitials associated with radiation damage, recombination of vacancies and interstitials, diffusion of vacancies and interstitials are considered in the model. With the model, we systematically simulate the influence of radiation conditions and thermodynamic properties on void migration mobility and growth kinetics.

* Corresponding author. Tel.: +1 509 371 6103.
E-mail address: yulan.li@pnl.gov (Y. Li).

0022-3115/$ - see front matter Published by Elsevier B.V.
doi:10.1016/j.jnucmat.2010.09.048

2. Description of the phase-field model

In this work, we study the effect of generation and recombination of point defects on void evolution in irradiated materials. It is well known that highly energetic fission fragments and neutrons initiate damage cascades, which generate a number of defects in nuclear fuel and cladding materials. Generally speaking, the defect formation energy, mobility, binding energy, and size distribution of the generated defects due to a cascade can be calculated using atomistic simulations. For simplicity, our phase-field model only considers the diffusion of single vacancies and single interstitials during irradiation. Mobile defect clusters, such as di-vacancies or small interstitial loops, are viewed as an assembly of individual vacancies or interstitials in this approach. Thus, they contribute to the overall defect concentrations and to the effective mobilities. In contrast, larger and immobile defect clusters are viewed as sinks or nucleation sites for defect clusters, which are assumed to affect the net generation rate of point defects. Therefore, two variables $c_{Vac}(\mathbf{r}, t)$ and $c_{Int}(\mathbf{r}, t)$ are used to describe the distribution of effective vacancies and interstitials, respectively. $\mathbf{r} = (r_1, r_2, r_3) = (x, y, z)$ and t are the spatial coordinate and time, respectively. It should be pointed out that the model can be extended to consider the diffusion of multiple defect clusters if more variables are employed. In the framework of the phase-field approach, the total free energy of the system including the chemical free energy and gradient energy is written as a function of $c_{Vac}(\mathbf{r}, t)$ and $c_{Int}(\mathbf{r}, t)$ as

$$E = \int_v \left[F(c_{Vac}, c_{Int}, T) + \frac{\kappa_{Vac}}{2}|\nabla c_{Vac}|^2 + \frac{\kappa_{Int}}{2}|\nabla c_{Int}|^2\right] dV \tag{1}$$

where $F(c_{Vac}, c_{Int}, T)$ is the chemical free energy, T is temperature, κ_{Vac} and κ_{Int} are the gradient energy coefficients of vacancy and interstitial concentrations, respectively. The diffusion of vacancies and interstitials are described by the Cahn–Hilliard equations [34]:

$$\begin{aligned}\frac{\partial c_{Vac}}{\partial t} &= \nabla \cdot \left[M_{Vac} \nabla \frac{\delta E}{\delta c_{Vac}}\right] + \xi(\mathbf{r}, t) + \dot{g}_{Vac}(\mathbf{r}, t) + \dot{\gamma}(\mathbf{r}, t) \\ &= \nabla \cdot \left[M_{Vac} \nabla \left(\frac{\partial F}{\partial c_{Vac}} - \kappa_{Vac} \nabla^2 c_{Vac}\right)\right] + \xi(\mathbf{r}, t) + \dot{g}_{Vac}(\mathbf{r}, t) + \dot{\gamma}(\mathbf{r}, t)\end{aligned} \tag{2}$$

$$\begin{aligned}\frac{\partial c_{Int}}{\partial t} &= \nabla \cdot \left[M_{Int} \nabla \frac{\delta E}{\delta c_{Int}}\right] + \zeta(\mathbf{r}, t) + \dot{g}_{Int}(\mathbf{r}, t) + \dot{\gamma}(\mathbf{r}, t) \\ &= \nabla \cdot \left[M_{Int} \nabla \left(\frac{\partial F}{\partial c_{Int}} - \kappa_{Int} \nabla^2 c_{Int}\right)\right] + \zeta(\mathbf{r}, t) + \dot{g}_{Int}(\mathbf{r}, t) + \dot{\gamma}(\mathbf{r}, t)\end{aligned} \tag{3}$$

where M_{Vac} and M_{Int} are the mobilities of vacancies and interstitials, respectively, which might be functions of defect concentration and temperature. $\xi(\mathbf{r}, t)$ and $\zeta(\mathbf{r}, t)$ are the thermal fluctuations of the vacancy and interstitial concentrations. $\dot{g}_{Vac}(\mathbf{r}, t)$ and $\dot{g}_{Vac}(\mathbf{r}, t)$ are the net generation rates of vacancies and interstitials, respectively. Vacancies and interstitials generated by fission fragments and/or neutron damage cascades can be absorbed by structural defects such as dislocations and grain boundaries. Therefore, the net increase of vacancies and interstitials depends on the generation rates of fission fragments and neutrons, hence the defect generation rates, and sink strengths, which are determined by the type and density of point defect sinks. Finally, $\dot{\gamma}(\mathbf{r}, t)$ is the recombination rate of vacancies and interstitials.

From Eqs. (2) and (3), it can be seen that the driving force of vacancy and interstitial diffusion includes the chemical potential gradients and the concentration gradients. They are derived by assuming that the microstructure evolution is driven by the minimization of the total free energy of the system. However, the microstructure evolution path depends on thermal fluctuation, defect generation, recombination, and defect sink interactions that occur in irradiated materials. If we compare the phase-field model with rate-theory [35], which is extensively used in predicting the microstructure evolution in irradiated materials, the phase-field model includes an additional driving force associated with the chemical potential gradient. In irradiated materials, the defect generation changes the local chemical potential, which should be one of the driving forces for microstructure evolution. In addition, a unique feature of the phase-field model is that it can provide three-dimensional microstructures and their evolution kinetics, which are the required thermodynamic and kinetic databases for larger scale simulations. We recently developed a number of phase-field models to predict the void lattice formation [28], gas bubble evolution [29], and void migration [20]. The results demonstrate the capability of phase-field approach in modeling the nonequilibrium process of microstructure evolution in irradiated materials. In the following, we discuss the thermodynamic and kinetic properties.

2.1. Chemical free energy

This work considers a model system, where voids and matrix containing vacancies and interstitials coexist. The void is viewed as a phase that consists 100% of vacancies. Therefore, the chemical free energy $F(c_{Vac}, c_{Int}, T)$ of the system presents a simple two phase equilibrium: the void phase with equilibrium concentrations $c_{Vac}^{eq} = 1.0$ and $c_{Int}^{eq} = 0.0$, and the matrix phase with equilibrium concentrations $c_{Vac}^{eq} = c_{Vac}^{eq0}(T)$ and $c_{Int}^{eq} = c_{Int}^{eq0}(T)$. The variables $c_{Vac}^{eq0}(T)$ and $c_{Int}^{eq0}(T)$ are the solubilities of vacancies and interstitials, respectively, in the matrix at temperature T. We take a defect-free system as the reference state, and assume its free energy is zero. Therefore, the free energy of a system with defects is the energy change from the defect-free system to the defected system. The regular solution model for the chemical free energy function [36] in two sublattices consisting of the host lattice and an interstitial lattice is used

$$F(c_{Vac}, c_{Int}, T) = F_1(c_{Vac}, T) + F_2(c_{Int}, T), \tag{4a}$$

$$\begin{aligned}F_1(c_{Vac}, T) = {} & k_B T[(1 - c_{Vac}) \ln(1 - c_{Vac}) + c_{Vac} \ln c_{Vac}] \\ & + b_4 c_{Vac}^4 + b_3 c_{Vac}^3 + b_2 c_{Vac}^2 + b_1 c_{Vac} + b_0,\end{aligned} \tag{4b}$$

$$F_2(c_{Int}, T) = k_B T[1 - c_{Int}) \ln(1 - c_{Int}) + c_{Int} \ln c_{Int}] + a c_{Int}. \tag{4c}$$

Since the vacancy concentration changes from zero to one while the thermal interstitial concentration is always close to zero, for simplicity, we ignore the interaction energy between vacancies and interstitials and assume that the equilibrium between voids and matrix depends only on the vacancy concentration. The interaction between vacancies and interstitials causes their recombination in the matrix and at void surfaces. We use a geometrically correct recombination rate to assure that all interstitials arriving at void surfaces recombine with vacancies so that the concentration of interstitials in the voids is zero. Thus, we separate the free energy into two parts, $F_1$and F_2. In Eqs. (4b) and (4c), k_B is the Boltzmann constant and T is the absolute temperature. The first part of Eqs. (4b) and (4c) is the ideal mixing entropy due to the vacancy or interstitial distribution in the matrix. The other terms are the enthalpy contributions to the free energy. The chemical free energy F_1 can be fitted by considering the following thermodynamic properties: (1) the equilibrium vacancy concentration c_{Vac}^{eq0} in the matrix; (2) the equilibrium vacancy concentration for the void phase, $c_{Vac}^{void} = 1.0$; (3) F_1 has a common tangent at c_{Vac}^{eq0} and c_{Vac}^{void}; (4) the spinodal point and (5) that $F_1(c_{Vac}^{eq0}, T)$ is temperature dependent. Fig. 1 displays the chemical free energy F_1 used in the simulations. The enthalpy part of the chemical free energy F_2 includes only the interstitial formation energy as expressed in Eq. (4c), where the coefficient a may depend on temperature. It should be noted that this free energy is constructed for a model system, but for a specific

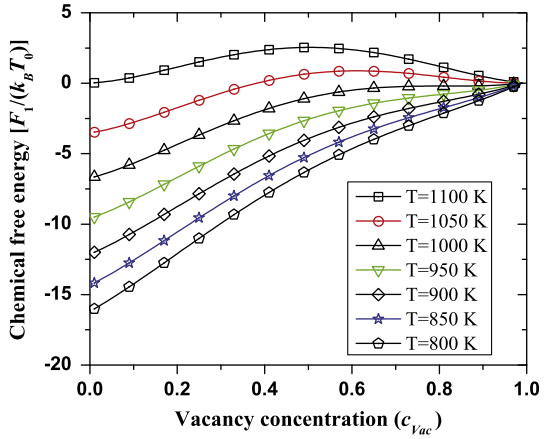

Fig. 1. Chemical free energy $F_1(c_{Vac}, T)$ used in the simulations, where T_0 = 1100 K.

material system more accurate free energy functions can be developed if we have accurate thermodynamic properties obtained from atomistic simulations, experiments, or/and thermodynamic calculations such as CALPHAD.

2.2. Generation and recombination rates of defects

In absence of any sinks for vacancies and interstitials, the net generation rates of vacancies and interstitials are completely determined by the damage rate $\dot{R}$. If we know the increase of vacancy concentration (N^R_{Vac}) and interstitial concentration (N^R_{Int}) including all the corresponding mobile clusters due to a particular irradiation event, the generation rates of vacancies and interstitials can be calculated as $\dot{g}^R_{Vac}(\mathbf{r}, t) = N^R_{Vac}\dot{R}$ and $\dot{g}^R_{Int}(\mathbf{r}, t) = N^R_{Int}\dot{R}$. However, in real materials there exist different sinks, such as dislocations and grain boundaries for vacancies and interstitials that affect the net vacancy and interstitial generation rates. In addition, fission fragment and neutron damage cascades are assumed to take place only in the matrix phase and not in voids. In the present work, the generation rates of vacancies and interstitials are described as $\dot{g}_{Vac}(\mathbf{r}, t) = \dot{g}^0_{Vac}H(c_{Vac})$ and $\dot{g}_{Int}(\mathbf{r}, t) = \dot{g}^0_{Int}H(c_{Vac})$, where $H(c_{Vac})$ is a smooth cut off function. It is 1.0 in the matrix phase, zero in voids, where the vacancy concentration is 1.0, and smoothly changes from 1.0 to 0 across the interface between the matrix and the voids. $\dot{g}^0_{Vac}$ and $\dot{g}^0_{Int}$ represent the net generation rates of vacancies and interstitials that depend on the N^R_{Vac}, N^R_{Int}, $\dot{R}$, and sink strengths ($\dot{g}^0_{Vac} \le \dot{g}^R_{Vac}$, $\dot{g}^0_{Int} \le \dot{g}^R_{Int}$). If the sink strengths change with time in irradiated materials, $\dot{g}^0_{Vac}$ and $\dot{g}^0_{Int}$ will also be time-dependent. For a given material and radiation conditions, these fundamental model parameters can be found in the rate-theory literature [35] and in Molecular Dynamic (MD) or Kinetic Monte Carlo (KMC) results [37–40]. In the present work, however, these parameters are given reasonable values that are varied to determine the resultant sensitivity. The recombination rate between vacancies and interstitials depends on the concentrations of both vacancies and interstitials, as well as their binding energy. The recombination rate in this work is described as $\dot{\gamma}(\mathbf{r}, t) = -\dot{\gamma}_0 c_{Vac}(\mathbf{r}, t)c_{Int}(\mathbf{r}, t)$, where $\dot{\gamma}_0$ is a model parameter related to diffusivity and the binding energy of vacancies and interstitials, such that the negative sign means that recombination reduces both vacancy and interstitial concentrations.

2.3. Numerical algorithm

For numerically solving Eqs. (2) and (3), the forward Euler marching scheme in time and the following normalizations are used: $r^*_i = \frac{r_i}{l_0}$, $t^* = \frac{k_BT_0M_0t}{l_0^2}$, $M^*_{Vac} = M_{Vac}/M_0$, $M^*_{Int} = M_{Int}/M_0$, $F^* = \frac{F}{k_BT_0}$, $\kappa^*_{Vac} = \frac{\kappa_{Vac}}{l_0^2k_BT_0}$, $\kappa^*_{Int} = \frac{\kappa_{Int}}{l_0^2k_BT_0}$, $\xi^* = \xi l_0^2/(k_BT_0M_0)$, $\zeta^* = \zeta l_0^2/(k_BT_0M_0)$, $\dot{g}^{0*}_{Vac} = \dot{g}^0_{Vac}l_0^2/(k_BT_0M_0)$, $\dot{g}^{0*}_{Int} = \dot{g}^0_{Int}l_0^2/(k_BT_0M_0)$ and $\dot{\gamma}^*_0 = \dot{\gamma}_0 l_0^2/(k_BT_0M_0)$ with l_0 and M_0 being the characteristic length and mobility, respectively, and T_0 being a given temperature, thus $\nabla = \left(\frac{\partial}{\partial r_1}, \frac{\partial}{\partial r_2}, \frac{\partial}{\partial r_3}\right) = \frac{1}{l_0}\left(\frac{\partial}{\partial r^*_1}, \frac{\partial}{\partial r^*_2}, \frac{\partial}{\partial r^*_3}\right) = \frac{1}{l_0}\nabla^*$. In reality, the mobilities M_{Vac} and M_{Int} may be different at the void surface and will depend on temperature. In the following calculations, constant mobility is assumed for the sake of simplicity. In order to improve the numerical stability and increase the time increment for the Cahn–Hilliard equations, we move the gradient terms from the right side of Eqs. (2) and (3) to the left side during time iterations:

$$\left\{c_{Vac} + \Delta t^*\kappa^*_{Vac}M^*_{Vac}\nabla^{*2}\nabla^{*2}c_{Vac}\right\}_{t^*+\Delta t^*} = \left\{c_{Vac} + \Delta t^*\left[M^*_{Vac}\nabla^{*2}\left(\frac{\partial F^*}{\partial c_{Vac}}\right) + \xi^* + \dot{g}^{0*}_{Vac}H(c_{Vac}) - \dot{\gamma}^*_0c_{Int}c_{Vac}\right]\right\}_{t^*}, \tag{5}$$

$$\left\{c_{Int} + \Delta t^*\kappa^*_{Int}M^*_{Int}\nabla^{*2}\nabla^{*2}c_{Int}\right\}_{t^*+\Delta t^*} = \left\{c_{Int} + \Delta t^*\left[M^*_{Int}\nabla^{*2}\left(\frac{\partial F^*}{\partial c_{Int}}\right) + \zeta^* + \dot{g}^{0*}_{Vac}H(c_{Vac}) - \dot{\gamma}^*_0c_{Int}c_{Vac}\right]\right\}_{t^*}, \tag{6}$$

We consider a simulation cell with periodic boundary conditions and solve Eqs. (5) and (6) in Fourier space [41]:

$$\tilde{c}_{Vac}(\mathbf{g}, t^* + \Delta t^*) = \frac{1}{1 + \kappa^*_{Vac}M^*_{Vac}g^4\Delta t^*}\left\{\tilde{c}_{Vac} + \Delta t^*\left[-M^*_{Vac}g^2\mathscr{F}\left(\frac{\partial F}{\partial c_{Vac}}\right) + \mathscr{F}(\xi^* + \dot{g}^{0*}_{Vac}H(c_{Vac}) - \dot{\gamma}c_{Int}c_{Vac})\right]\right\}_{(\mathbf{g},t^*)} \tag{7}$$

$$\tilde{c}_{Int}(\mathbf{g}, t^* + \Delta t^*) = \frac{1}{1 + \kappa^*_{Int}M^*_{Int}g^4\Delta t^*}\left\{\tilde{c}_{Int} + \Delta t^*\left[-M^*_{Int}g^2\mathscr{F}\left(\frac{\partial F}{\partial c_{Int}}\right) + \mathscr{F}(\zeta^* + \dot{g}^{0*}_{Int}H(c_{Int}) - \dot{\gamma}c_{Int}c_{Vac})\right]\right\}_{(\mathbf{g},t^*)}, \tag{8}$$

where $\mathscr{F}$ refers to the Fourier transform over the real space vector $\mathbf{r}$, $\mathbf{g}$ is a reciprocal vector in the Fourier space and $g^2 = \mathbf{g}\cdot\mathbf{g}$. After solving $\tilde{c}_{Vac}$ and $\tilde{c}_{Vac}$, the inverse Fourier transforms on $\tilde{c}_{Vac}$ and $\tilde{c}_{Vac}$ will give the distribution of c_{Vac} and c_{Int} in real space, thus, the microstructure.

3. Results and discussion

The main objectives of this work are to (1) develop a phase-field model and (2) to parametrically study the effect of radiation conditions and thermodynamic properties on void migration as well as void growth kinetics. In the simulations, we vary the following parameters: the vacancy concentration in the matrix, the defect generation rate, and the recombination rate between vacancies and interstitials. All the simulations are carried out in two dimensions even though the formulas and codes are developed for 3D. The simulation cell has a length of $L_x = 256l_0$ in $x = r_1$ direction, and $L_y = 256l_0$ in $y = r_2$ direction, as a representative area in a fuel. Periodic boundary conditions were employed for both x and y directions. The given initial uniform concentrations of vacancies and interstitials in the matrix are c^0_{Vac} and c^0_{Int}, respectively. A temperature field of

$$T = \begin{cases} T_1 + \frac{T_2 - T_1}{2}\left[\cos\left(\frac{r}{R_0}\right)\pi + 1\right], & r \le R_0, \\ T_1, & r > R_0, \end{cases} \quad (9)$$

is applied to the simulation cell, where $R_0 = 115l_0$, $T_1 = 900$ K, $T_2 = 920$ K and $r = 0$ is the center of the simulation cell. The temperature field is centrally symmetric and smoothly satisfies the periodic conditions. In addition, the temperature field provides a region at $r = R_0/2$, where the temperature gradient is nearly a constant. In the following simulations, the void growth and migration kinetics are analyzed in that region.

The mobility of vacancies and interstitials strongly depends on the material. In UO_2 the vacancy mobility is larger than that of interstitials while interstitials typically have higher mobilities in cladding materials. For simplicity the interstitial mobility is set equal to that of vacancies, i.e., $M^*_{Int} = M^*_{Vac} = 1.0$. In addition, a ratio between the net generation rates of $\dot{g}^{0*}_{Int}/\dot{g}^{0*}_{Vac} = 0.01$ is used, which implies that most interstitials segregate rapidly to sinks other than voids. Although this simplified model only considers voids as sinks, a full treatment of irradiation damage must consider all appropriate defect sinks, such as grain boundaries, line dislocations, dislocation loops, and defect clusters. In the following calculations, a normalized time step $\Delta t^* = 0.0001$ is used. The thermal fluctuations of the vacancy concentration and interstitial concentration in Eqs. (7) and (8) are ignored because our focus is on the irradiation induced microstructure evolution.

3.1. Soret effect

The Soret effect or Ludwig–Soret effect [42], also called thermophoresis or thermomigration or thermodiffusion, is a phenomenon in which a temperature gradient in a mixture of substances gives rise to a concentration gradient. To verify if our model is able to describe the Soret effect, simulations with initial uniform vacancy and interstitial concentrations in a temperature field are carried out. The temperature field is given by Eq. (9). The initial vacancy and interstitial concentrations in the matrix are $c^0_{Vac} = 0.02$ and $c^0_{Int} = 0.0002$, respectively. Fig. 2 shows the equilibrium concentration contours. The colored background in the figures is the temperature field. From Fig. 2a, it is seen that vacancies preferentially migrate to the higher temperature causing a vacancy concentration

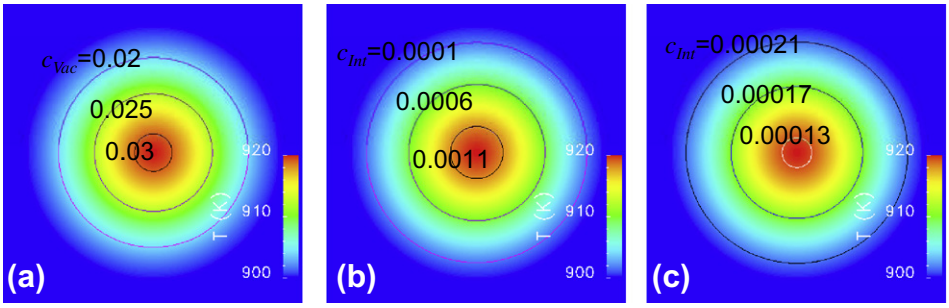

Fig. 2. Vacancy and interstitial gradients resulted from the gradient of temperature. (a) Contours of vacancy concentration c_{Vac}; (b) contours of interstitial concentration c_{Int} when $a_1 = 0$ and (c) contours of interstitial concentration c_{Int} when $a_1 = 6$.

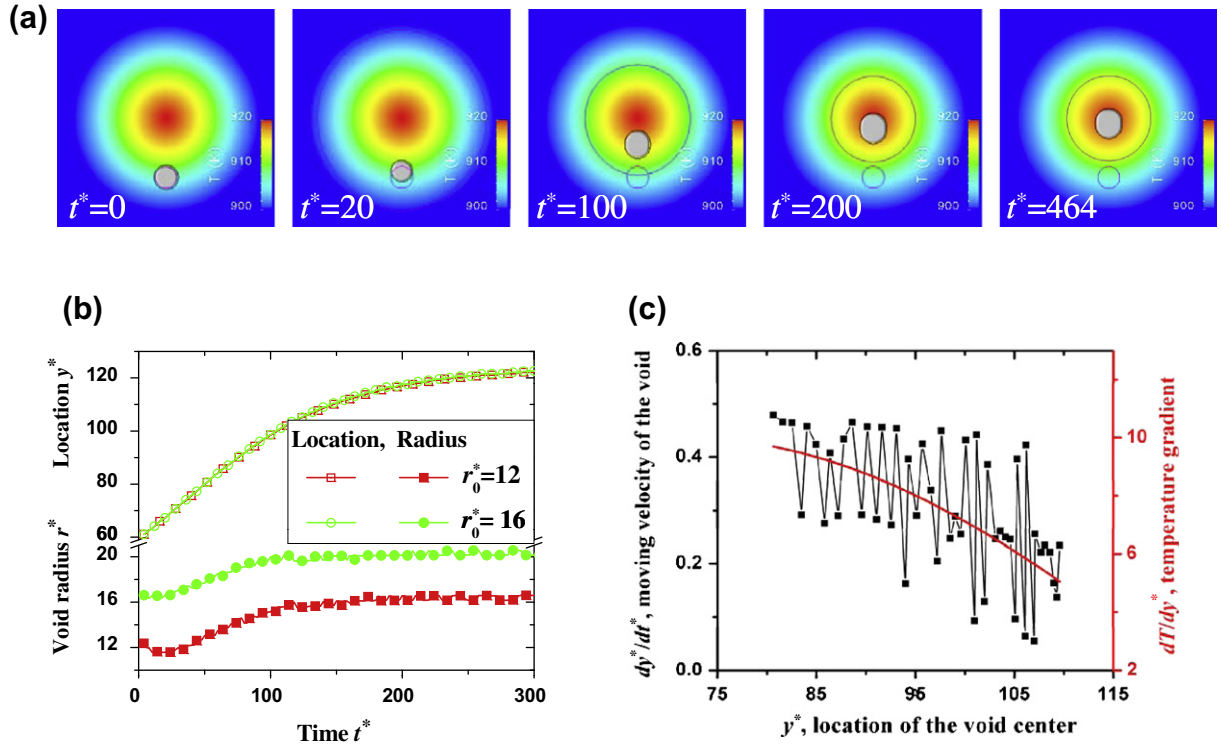

Fig. 3. (a) Void migration and growth with time; (b) void center location and void radius versus time for voids with different initial sizes and (c) void migration mobility in the given temperature gradient.

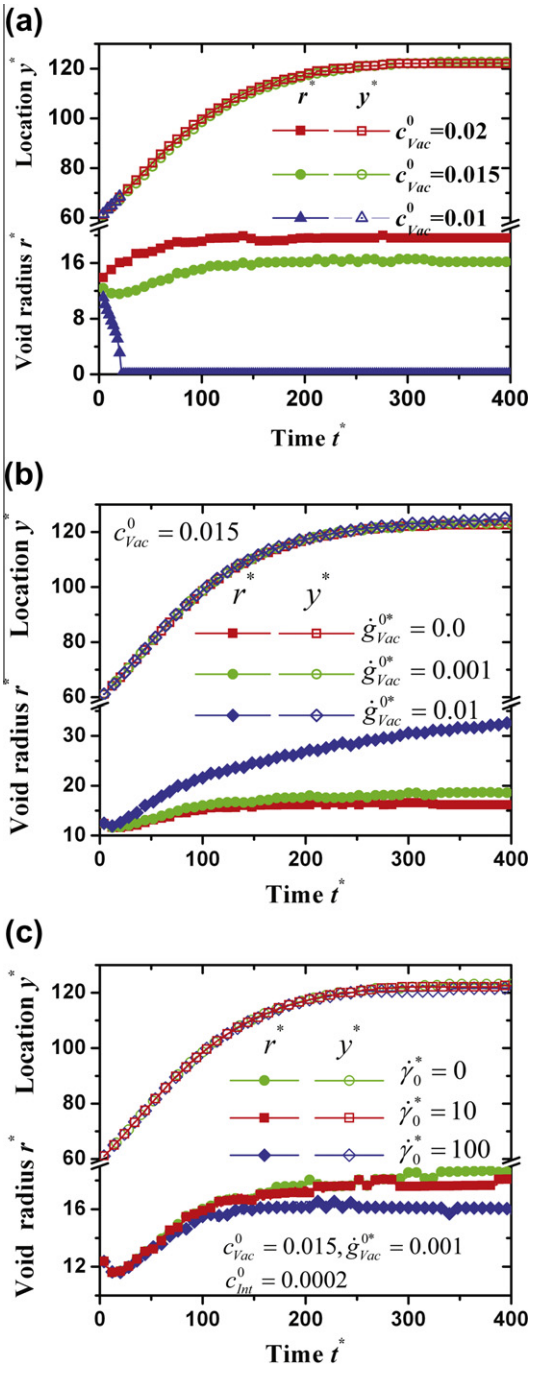

Fig. 4. Effects of (a) vacancy concentration; (b) vacancy generation rate and (c) recombination rate on void growth and migration.

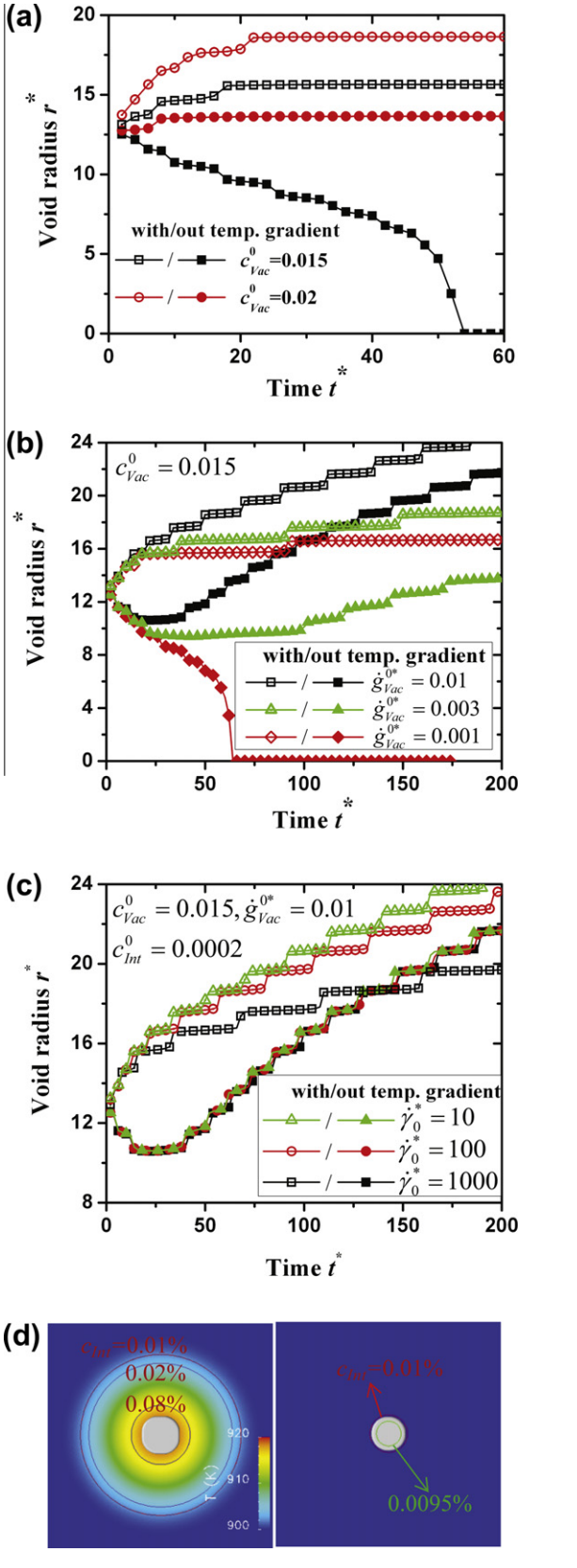

Fig. 5. Dependence of void growth on the combined effect of temperature gradient and (a) vacancy concentration; (b) vacancy generation rate; (c) recombination rate. (d) morphologies of void and interstitial distribution with/without temperature gradient for the case with $c^0_{Vac}=0.015$, $c^0_{Int}=0.0002, \dot{g}^{0*}_{Vac}=0.01$, $\dot{\gamma}^*_0=100.0$, and $t^*=150$.

gradient to develop. If one assumes the formation energy coefficient a in Eq. (4c) is linearly dependent on temperature in a form of $a = a_0 + a_1 k_B T$, the simulations show that interstitials migrate down to lower temperature when $a_1 > 4.0$, and interstitials migrate up to higher temperature when $a_1 \leqslant 4.0$ as shown in Fig. 2b and c. With the $a_1 = 4.0$, we can estimate that formation energy change is about 0.34 eV from 0 K to 1000 K. Fig. 2 demonstrates that the Soret effect is taken into account in our model. Whether the interstitials migrate up or down with the temperature gradient depends on the chemical potentials of the interstitials. In the following simulations, $a_1 = 0$ is used so that the interstitials preferentially migrate to higher temperatures.

3.2. Void migration and migration mobility

Consider a single preexisting void in the given temperature field. The void may have formed during fabrication or service. Similar to vacancies, the void migrates to higher temperatures and grows with time as illustrated in Fig. 3a, where $c^0_{Vac} = 0.015$, $\dot{g}^{0*}_{Vac} = 0$, $\dot{\gamma}^*_0 = 0$, and the void initial radius $r^*_0 = 12$. In the figures, the colored background is the temperature field as given by Eq. (9) and the solid grey circle is the void. The small open circle displays the initial void size and location. The big circle is the vacancy concentration contour with $c_{Vac} = 0.015$. The circle around the void is the contour with $c_{Vac} = 0.1$. Since the center of the simulation cell is at the highest temperature, the void migrates to the center and stops. But it continues growing until the vacancies reach their equilibrium distribution in the given temperature field. It is observed that the void elongates along the temperature gradient direction during its migration and growth. When it arrives at the center of the simulation cell, it reverts to a circular shape due to the isotropic interfacial energy we assumed.

Fig. 3b plots the void center location and radius changing with time and y^* is measured from the bottom of the simulation cell to the void center along the line connecting the void center to the simulation cell center. The radius is also measured along the same line. It is found that the considered voids with different initial sizes shrink at the beginning, then grow, and finally migrate with almost constant sizes. The initial shrinking of the voids is due to the modification of void surface because initially the assumed void does not have the lowest interface energy. The subsequent growth of the void is because of the supersaturation of vacancies caused by the vacancy generation. After the vacancy concentration establishes its equilibrium distribution in the given temperature field void growth stops and it migrates to the higher temperature. Void center locations as a function of time are plotted in Fig. 3b. It can be seen that the position of void centers with different sizes move with the same velocity during their migration, which implies that the migration mobility is independent of the void size, thus agreeing with the theoretical prediction of bulk diffusion controlled migration [15]. The migration velocity of the voids is shown in Fig. 3c. The velocity is calculated with dy^*/dt^*. The scatter in the velocity is due to an error bar of $0.5l_0$ for calculating y^*. The thick solid line is the temperature gradient used in the simulation. One can see the void migration velocity or mobility decreases with decreasing temperature gradient.

The simulations demonstrate void migration to the high temperature regions, which can explain the formation of the observed central hole in spent nuclear fuel. However, in nuclear fuel there also exists a void microstructure with particular size and spatial distributions, which were not considered here. To more accurately evaluate the central hole formation kinetics, large-scale, 3D simulations are required. However, with our current computer resources this phase-field model cannot achieve the required length and time scales. As shown above, phase-field modeling can obtain the mobility of a single void in a given temperature field. A complete database of void growth and migration mobility could be developed to be used as inputs to macro-scale simulations for predicting the structure and properties evolution such as central hole formation in nuclear fuels, but this is beyond the present scope of this paper. The accuracy of the phase-field simulation results are completely determined by the thermodynamic and kinetic properties used in the simulations, such as the chemical free energy of the solid with vacancies and interstitials, surface energy of voids, and mobility of vacancies and interstitials. A direct comparison of void migration velocities obtained from phase-field modeling and experiments can validate both the phase-field model and the thermodynamic and kinetic properties used in the simulations.

3.3. Effect of vacancy concentration c^0_{Vac}, vacancy generation rate $\dot{g}^{0*}_{Vac}$, and defect recombination rate $\dot{\gamma}^*_0$ on void migration and growth

Fig. 4a–c shows the effect of the vacancy concentration c^0_{Vac} in the matrix, vacancy generation rate $\dot{g}^{0*}_{Vac}$, and the recombination rate $\dot{\gamma}^*_0$ between vacancies and interstitials on void migration and growth. The initial radius of the void was $r^*_0 = 12$. As expected, void stability and growth kinetics depend on the vacancy concentration when the vacancy generation rate is zero. From Fig. 4a it can be seen that when the vacancy concentration is lower than the assumed solubility the void shrinks, and disappears after some time. Increasing the vacancy concentration ($c^0_{Vac} = 0.015, 0.02$) stabilizes the preexisting void, and initiates void growth. Fig. 4b plots the effect of generation rate on void migration and growth kinetics. It is clear that void growth increases with increasing vacancy generation rates. When the initial vacancy concentration and vacancy generation rate are fixed, the effect of the recombination rate $\dot{\gamma}^*_0$ on void migration and growth is demonstrated by Fig. 4c, where $c^0_{Vac} = 0.015, c^0_{Int} = 0.0002$, and $\dot{g}^{0*}_{Vac} = 0.001$. One can see that increased recombination of vacancies and interstitials decreases void growth, which is an obvious result because recombination of vacancies and interstitials reduces the vacancy concentration in the matrix. If the recombination takes place at the void surface, it leads to a decrease in void size. If we compare the curves of void location versus time in Fig. 4a–c, we conclude that void migration mobility is independent of vacancy concentration, vacancy generation rate, and recombination rate. From these results, we also conclude that the parameters: vacancy concentration, vacancy generation rate, and recombination rate strongly affect void growth kinetics, which results in a change of void sizes. However, void migration is independent of void size since void migration is controlled by bulk diffusion.

3.4. Central void growth with/without temperature gradient

The central hole growth may result both from a continuous supply of small voids and vacancies. The simulations above show that a void migration mobility can be obtained which is important for predicting the central hole growth kinetics in macro-scale simulations. In this section we examine how the temperature gradient affects the central void growth through vacancy diffusion. To do this, a void is set at the center of the simulation cell. The void does not move even in the presence of a temperature gradient since the center is at the highest temperature. With and without a temperature gradient, the dependency of changes in void radii on the vacancy concentration, vacancy generation rate, and recombination rate are shown in Fig. 5a–c. Fig. 5a and b shows that temperature gradients stabilize small voids and increase void growth compared to the same vacancy concentration and same vacancy generation rate without a temperature gradient. This is because the temperature gradient causes a vacancy flux, the Soret effect, which provides additional vacancies at the center of the simulation cell. However, the temperature gradient also results in an interstitial flux. Fig. 5c shows that the recombination rate does not affect void growth without a temperature gradient while void growth decreases with increasing recombination rate under a temperature gradient since the interstitial flux recombines with the vacancy flux and fewer vacancies reach the void.

4. Conclusions

We have developed a phase-field model for studying the effect of temperature gradients, vacancy concentrations, vacancy generation rates, and the recombination of vacancies and interstitials on void migration and growth in materials during irradiation. We

observed the Soret effect as expected due to thermally-induced concentration gradients of point defects such that void migration to higher temperatures is predicted. It is found that void migration mobility is independent of void size and considered parameters, such as the vacancy concentration, the vacancy generation rate, and the recombination rate, with the assumption of bulk diffusion controlled void migration. Void migration mobility is predicted to be dependent on the temperature gradient and decreases with decreasing temperature gradient. Void growth is influenced by all the considered parameters including the vacancy concentration, the vacancy generation rate, and the recombination rate. A temperature gradient causes vacancies, interstitials, and voids to flow from lower temperature regions to higher temperature regions, which could result in central hole formation in spent nuclear fuel. The simulations demonstrated that the developed phase-field model is able to evaluate the effects of the thermodynamic and kinetic properties of a material system on void migration and growth kinetics. However, quantitative phase-field simulations require accurate thermodynamic and kinetic properties of the corresponding system. Lacking thermodynamic and kinetic properties, however, the phase-field simulations can use reasonable thermodynamic and kinetic properties which could be obtained from experiments and atomistic simulations, to build up a thermodynamic database on how the thermodynamic and kinetic properties affect the void migration and growth. Such a database is important for uncertainty evaluation of both mesoscale and macro-scale simulations.

Acknowledgment

This research was supported by the US Department of Energy's Nuclear Energy Advance Modeling and Simulation (NEAMS) Program in Pacific Northwest National Laboratory, which is operated by Battelle Memorial Institute for the US Department of Energy under Contract No. DE-AC05-76RL01830.

References

[1] S.L. Sass, B.L. Eyre, Philos. Mag. 27 (1973) 1447.
[2] K. Une, K. Nogita, S. Kashibe, M. Imamura, J. Nucl. Mater. 188 (1992) 65.
[3] S. Kashibe, K. Une, K. Nogita, J. Nucl. Mater. 206 (1993) 22.
[4] I. Zacharie, S. Lansiart, P. Combette, M. Trotabas, M. Coster, M. Groos, J. Nucl. Mater. 255 (1998) 92.
[5] K. Katsuyama, T. Nagamine, S. Matsumoto, M. Ito, J. Nucl. Sci. Technol. 39 (2002) 804.
[6] K. Katsuyama, T. Nagamine, S. Matsumoto, M. Ito, J. Nucl. Sci. Technol. 40 (2003) 220.
[7] D. Faulkner, C.H. Woo, J. Nucl. Mater. 90 (1980) 307.
[8] D.S. Gelles, J. Nucl. Mater. 225 (1995) 163.
[9] G.W. Greenwood, M.V. Speight, J. Nucl. Mater. 10 (1963) 140.
[10] S.L. Dudarev, A.A. Semenov, C.H. Woo, Phys. Rev. B 67 (2003) 094103.
[11] A.S. Gontar, R.Y. Kucherov, M.V. Nelidov, Sov. Atom. Energy 58 (1985) 64.
[12] E.E. Gruber, J. Appl. Phys. 38 (1967) 243.
[13] F.A. Nichols, J. Nucl. Mater. 27 (1968) 137.
[14] F.A. Nichols, J. Nucl. Mater. 30 (1969) 143.
[15] P.G. Shewmon, Jom–J. Met. 16 (1964) 753.
[16] L.J. Perryman, P.J. Goodhew, Acta Metall. 36 (1988) 2685.
[17] V. Tikare, E.A. Holm, J. Am. Ceram. Soc. 81 (1998) 480.
[18] V.I. Dubinko, A.A. Turkin, Appl. Phys. A – Mater. Sci. Process. 58 (1994) 21.
[19] H. Trinkaus, B.N. Singh, J. Nucl. Mater. 307 (2002) 900.
[20] S.Y. Hu, C.H. Henager, Acta Mater. 58 (2010) 3230.
[21] A. Karma, W.J. Rappel, Phys. Rev. E 57 (1998) 4323.
[22] Y.L. Li, S.Y. Hu, Z.K. Liu, L.Q. Chen, Acta Mater. 50 (2002) 395.
[23] S.G. Kim, W.T. Kim, T. Suzuki, Phys. Rev. E 60 (1999) 7186.
[24] Y.M. Jin, A. Artemev, A.G. Khachaturyan, Acta Mater. 49 (2001) 2309.
[25] Y.M. Jin, A.G. Khachaturyan, Philos. Mag. Lett. 81 (2001) 607.
[26] H.C. Yu, W. Lu, Acta Mater. 53 (2005) 1799.
[27] M. Stan, J.C. Ramirez, P. Cristea, S.Y. Hu, C. Deo, B.P. Uberuaga, S. Srivilliputhur, S.P. Rudin, J.M. Wills, J. Alloy Compd. 444 (2007) 415.
[28] S.Y. Hu, C.H. Henager, J. Nucl. Mater. 394 (2009) 155.
[29] S.Y. Hu, C.H. Henager, H.L. Heinisch, M. Stan, M.I. Baskes, S.M. Valone, J. Nucl. Mater. 392 (2009) 292.
[30] S. Rokkam, A. El-Azab, P. Millett, D. Wolf, Model Simul. Mater. Sci. Eng. 17 (2009) 18.
[31] S.Y. Hu, M.I. Baskes, M. Stan, Appl. Phys. Lett. 90 (2007) 081921.
[32] X.H. Guo, S.Q. Shi, X.Q. Ma, Appl. Phys. Lett. 87 (2005) 221910.
[33] A. Karma, D.A. Kessler, H. Levine, Phys. Rev. Lett. 87 (2001) 045501.
[34] J.W. Cahn, Acta Metall. 9 (1961) 795.
[35] C.J. Ortiz, M.J. Caturla, Phys. Rev. B 75 (2007) 184101.
[36] U.R. Kattner, Jom–J. Miner Met. Mater. Soc. 49 (1997) 14.
[37] D.J. Bacon, F. Gao, Y.N. Osetsky, J. Nucl. Mater. 276 (2000) 1.
[38] A. Souidi, C.S. Becquart, C. Domain, D. Terentyev, L. Malerba, A.F. Calder, D.J. Bacon, R.E. Stoller, Y.N. Osetsky, M. Hou, J. Nucl. Mater. 355 (2006) 89.
[39] C. Domain, C.S. Becquart, L. Malerba, J. Nucl. Mater. 335 (2004) 121.
[40] K.L. Wong, H.J. Lee, J.H. Shim, B. Sadigh, B.D. Wirth, J. Nucl. Mater. 386 (2009) 227.
[41] L.Q. Chen, J. Shen, Comput. Phys. Commun. 108 (1998) 147.
[42] J.K. Platten, J. Appl. Mech. – Trans. ASME 73 (2006) 5.